Modulation of apoptotic response by LAR family phosphatases–cIAP1 signaling during urinary tract morphogenesis

Katherine Stewart[a,b], You Chi Tang[a,b], Maxwell E. R. Shafer[a,b], Adda-Lee Graham-Paquin[a,b], and Maxime Bouchard[a,b,1]

[a]Department of Biochemistry, McGill University, Montreal, QC, Canada H3G 1Y6; and [b]Goodman Cancer Research Centre, McGill University, Montreal, QC, Canada H3A 1A3

Edited by Marianne Bronner, California Institute of Technology, Pasadena, CA, and approved September 14, 2017 (received for review May 2, 2017)

The elimination of unwanted cells by apoptosis is necessary for tissue morphogenesis. However, the cellular control of morphogenetic apoptosis is poorly understood, notably the modulation of cell sensitivity to apoptotic stimuli. Ureter maturation, the process by which the ureter is displaced to the bladder wall, represents an exquisite example of morphogenetic apoptosis, requiring the receptor protein tyrosine phosphatases (RPTPs): LAR and RPTPσ. Here we show that LAR-RPTPs act through cellular inhibitor of apoptosis protein 1 (cIAP1) to modulate caspase 3,7-mediated ureter maturation. Pharmacologic or genetic inactivation of cIAP1 reverts the apoptotic deficit of LAR-RPTP–deficient embryos. Moreover, *Birc2* (cIAP1) inactivation generates excessive apoptosis leading to vesicoureteral reflux in newborns, which underscores the importance of apoptotic modulation during urinary tract morphogenesis. We finally demonstrate that LAR-RPTP deficiency increases cIAP1 stability during apoptotic cell death. Together these results identify a mode of cIAP1 regulation playing a critical role in the cellular response to apoptotic pathway activation in the embryo.

apoptosis | cIAP1 | LAR receptor protein tyrosine phosphatases | urinary tract morphogenesis | vesicoureteral reflux

Apoptotic cell death is necessary for normal embryo development (1–4). As tissues take shape, the appropriate response of a cell to apoptosis is crucial as both excessive and insufficient apoptotic cell death can have detrimental effects on tissue morphogenesis. However, the molecular mechanisms underlying this decision are still largely elusive.

Morphogenetic apoptosis has been shown to play an important role during urinary tract development. Following kidney induction by ureter budding from the nephric duct, the base of the ureter must be displaced to its final location in the bladder epithelium by apoptosis-mediated removal of the intervening common nephric duct (CND) (5–8). A failure in this process leads to ureter obstruction and renal damage (6, 7). In humans, ureter obstruction, vesicoureteral reflux (VUR) and other developmental defects of the urinary tract are part of the disease group congenital anomalies of the kidney and urinary tract (CAKUT), which underlies a large part of pediatric renal failures worldwide (9).

Apoptotic cell death results from the activation of caspases, which are evolutionarily conserved cysteine-dependent aspartyl proteases synthesized as inactive zymogens (10). Upon apoptotic pathway stimulation, caspases 8 and/or 9 activate effector caspases 3 and 7, thereby promoting widespread proteolytic damage and subsequent cellular dismantling. Caspase-dependent apoptosis is held in check by members of the inhibitor of apoptosis protein (IAP) family, namely, X-linked IAP (XIAP) and cellular IAPs (cIAP1 and cIAP2), characterized by amino-terminal BIR domains mediating protein–protein interactions, and a carboxyl-terminal RING domain with E3-ligase activity (11). Notably, by acting as E3-ubiquitin ligases, IAPs are capable of promoting the ubiquitination and proteosomal degradation of themselves and several binding partners. IAP activity can also be relieved by binding of mitochondrially released Smac (also known as Diablo) to the IAP proteins (12–15). This neutralization event occurs via the BIR domains of IAPs, effectively occluding caspase interaction sites and facilitating caspase 3 and 7 activation (16–18). How the balance between IAPs and Smac dictates apoptotic morphogenesis during embryonic development, and the potential contribution to congenital disease, however, is unclear.

We previously identified the LAR family receptor protein tyrosine phosphatases (RPTPs), LAR and RPTPσ, as required for apoptosis-mediated elimination of the CND (7). Here, we demonstrate the critical role of cIAP1 in the regulation of ureter maturation downstream of LAR family phosphatases. In absence of cIAP1, ureter maturation is accelerated, leading to vesicoureteral reflux.

Results

LAR-RPTPs Regulate Caspase 3-Dependent Apoptosis in Fibroblasts. To better understand the molecular mechanism of apoptotic regulation by LAR-RPTPs, we used mouse embryonic fibroblasts (MEFs) derived from animals lacking all three members of the family [*Ptprs*$^{-/-}$; *Ptprf*$^{-/-}$; *Ptprd*$^{-/-}$ triple knockout (TKO)]. Remarkably, fibroblasts lacking LAR-RPTPs showed a marked delay in apoptotic cell death, in sharp contrast to the quick response of wild-type (WT) MEFs, as assessed by TUNEL staining and activation of a fluorogenic caspase 3/7 substrate (Fig. 1 *A* and *B* and *SI Appendix*, Fig. S1*A*). While cleaved caspase 3 failed to accumulate in response to the intrinsic apoptotic stimulus cisplatin, upstream caspase 9 underwent normal catalytic cleavage (Fig. 1*C*). Accordingly, TKO cells showed normal levels of

Significance

Apoptotic morphogenesis requires strict regulation as both excessive and insufficient cell death is detrimental to tissue function. Here we use the process of ureter maturation, wherein the ureter connects to the bladder by the apoptosis-mediated removal of the intervening common nephric duct (CND), to investigate this paradigm. We find that LAR family phosphatases antagonize cIAP1 activity by decreasing its stability, thereby releasing the brake on CND elimination. In addition, we demonstrate that *Birc2* (cIAP1) mutant embryos exhibit increased CND apoptosis, leading to accelerated ureter maturation and vesicoureteral reflux. Together this highlights the importance of modulating the rate of apoptosis during morphogenesis, which may act as a morphogenetic timer to allow for appropriate tissue rearrangements during embryonic development.

Author contributions: K.S. and M.B. designed research; K.S., Y.C.T., M.E.R.S., and A.G.-P. performed research; K.S., Y.C.T., M.E.R.S., A.G.-P., and M.B. analyzed data; and K.S. and M.B. wrote the paper.

The authors declare no conflict of interest.

This article is a PNAS Direct Submission.

Published under the PNAS license.

[1]To whom correspondence should be addressed. Email: maxime.bouchard@mcgill.ca.

This article contains supporting information online at www.pnas.org/lookup/suppl/doi:10.1073/pnas.1707229114/-/DCSupplemental.

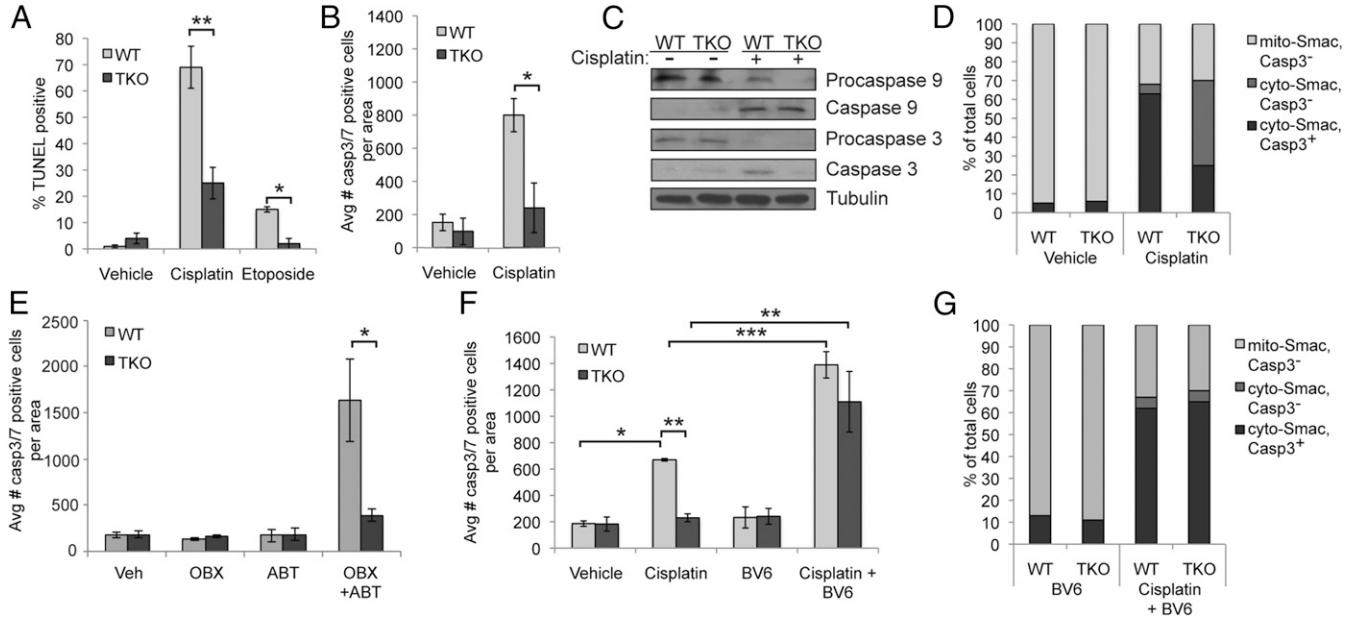

Fig. 1. LAR family phosphatases regulate caspase 3-dependent apoptosis through cIAPs. (*A*) *Ptprs; Ptprf; Ptprd* triple knockout (TKO) MEF lines (n = 4 independent cell lines, with a minimum of 500 cells per condition) are resistant to intrinsic (cisplatin, etoposide) apoptotic triggers as revealed by TUNEL and DAPI stainings. (*B*) TKO MEFs fail to activate caspase 3 in response to cisplatin treatment. The amount of caspase activity was tracked temporally with a fluorogenic caspase 3,7-substrate by live cell imaging. A representative analysis at 18 h is shown. (*C*) Immunoblots of WT and TKO MEFs show that LAR-RPTP–deficient MEFs cleave upstream caspase 9 normally but fail to accumulate cleaved caspase 3 in response to 6-h stimulation with cisplatin. (*D*) Live cell imaging of MEFs transfected with a mitochondrially localized Smac-RFP construct (mito-Smac) in the presence of a fluorogenic caspase 3,7-substrate reveals normal release of Smac after 4 h of cisplatin stimulation (cyto-Smac), which is accompanied by an increase in caspase 3,7 activity ($Casp3^+$) in WT but not TKO MEFs (200–500 cells per condition). (*E*) Mitochondrial outer membrane permeabilization triggered by 4-h treatment with the anti-apoptotic Bcl2-family inhibitors obatoclax (OBX) and ABT-737 (ABT) reveals that TKO MEFs are blocked in caspase 3,7 activation downstream of Bax/Bak-mediated MOMP. (*F*) Inactivation of IAPs by the Smac-mimetic BV6 (5 μM) restores caspase 3,7 activity in TKO MEFs upon cisplatin stimulation. (*G*) BV6-mediated rescue of TKO MEF apoptosis occurs downstream of mitochondrial Smac release. Imaging of MEFs transfected with a Smac-RFP construct in the presence of a fluorogenic caspase 3,7-substrate reveals normal release of Smac into the cytosol in response to cotreatment with BV6 and cisplatin (200–500 cells per condition). All experiments shown are representative of four independent experiments, performed in technical triplicates. All P values are calculated using one-way ANOVA. All error bars indicate SEM. $^*P < 0.05$, $^{**}P < 0.01$, $^{***}P < 0.005$.

mitochondrial outer membrane permeabilization (MOMP) as assessed by release of tagged Smac (Fig. 1*D* and *SI Appendix*, Fig. S1*B*). To validate that LAR family phosphatases act downstream of mitochondrial permeabilization, we triggered apoptotic cell death at the mitochondrial level by short-term addition of the BH3-mimetics ABT-737 (Bcl-2 inhibitor) and obatoclax (Mcl-1 inhibitor), which produced a blunted apoptotic response in TKO MEFs similar to that observed with cisplatin treatment (Fig. 1*E*). Collectively, these results point to a role for the LAR-RPTPs in regulating caspase 3 downstream of mitochondrial permeabilization and caspase 9 activation.

This conclusion suggested a possible role of the Smac-IAP pathway in the apoptotic resistance of LAR family-deficient cells. To test this, we used a small molecule Smac mimetic (BV6) that acts as an inhibitor of cIAP1, cIAP2, and, to a lesser extent, XIAP (19, 20). In line with a role for IAP activity in restricting the response to intrinsic apoptotic stimuli, cotreatment of wild-type fibroblasts with cisplatin and BV6 resulted in an increase in caspase 3 activity (Fig. 1 *F* and *G* and *SI Appendix*, Fig. S1*C*). Strikingly, IAP inactivation by BV6 in TKO fibroblasts completely restored their ability to activate caspase 3 and fully execute apoptosis in response to cisplatin without altering upstream mitochondrial permeabilization dynamics (Fig. 1 *F* and *G* and *SI Appendix*, Fig. S1 *C* and *D*). Similarly, BV6-mediated IAP elimination was able to resensitize TKO MEFs to apoptotic cell death triggered by ABT-737 and obatoclax (*SI Appendix*, Fig. S1*E*).

In MEFs, the extrinsic stimulus TNFα/cycloheximide (TNFα/CHX) triggers caspase-dependent apoptotic cell death through the mitochondrial pathway. In line with the results above, TNFα/CHX stimulation of TKO MEFs led to normal cleavage of caspase 8, activation of tBid, and release of mitochondrial SMAC, but failed to accumulate active caspase 3 (*SI Appendix*, Fig. S1 *F–I*). In addition, elimination of IAP activity through BV6 treatment completely restored apoptotic sensitivity in LAR phosphatase-deficient cells treated with TNFα/CHX (*SI Appendix*, Fig. S1*J*). Collectively, these results implicate the LAR family phosphatases in the regulation of IAP activity downstream of MOMP in response to both intrinsic and extrinsic apoptotic death stimuli.

IAP Activity Is Required for Apoptosis-Mediated Ureter Maturation. In the embryo, ureter maturation serves to separate the urinary and genital tracts by regulated apoptotic elimination of the entire CND (6, 7, 21, 22). To investigate whether LAR-RPTPs act through IAPs during ureter maturation, we adapted an ex vivo organ culture approach (6) using $Pax2BAC^{GFP}$ transgenic embryos to visualize the renal lineages (Fig. 2*A*). Notably, the rate of CND elimination over the first 24 h in organ culture (early phase) closely parallels the initial rate of ureter maturation that occurs in vivo (Fig. 2 *A* and *B*), validating the relevance of the system. We then treated WT ex vivo cultures with the Smac mimetic BV6, which resulted in a twofold acceleration of CND elimination (Fig. 2 *C* and *D*), suggesting a functional role for IAPs during ureter maturation. Addition of the caspase 3,7 inhibitor z-DEVD-fmk in either the presence or absence of BV6 abrogated CND elimination (Fig. 2 *C* and *D*), demonstrating that both normal and BV6-accelerated ureter maturation occur via apoptotic cell death.

cIAP1 Mediates LAR-RPTP–Dependent Apoptosis During Ureter Maturation. We next asked whether the reduction in CND apoptosis observed in $Ptprs^{-/-}; Ptprf^{-/-}$ [double knockout (DKO)] embryos (7) (Fig. 3*A*) resulted from sustained IAP activity, as was observed in MEFs.

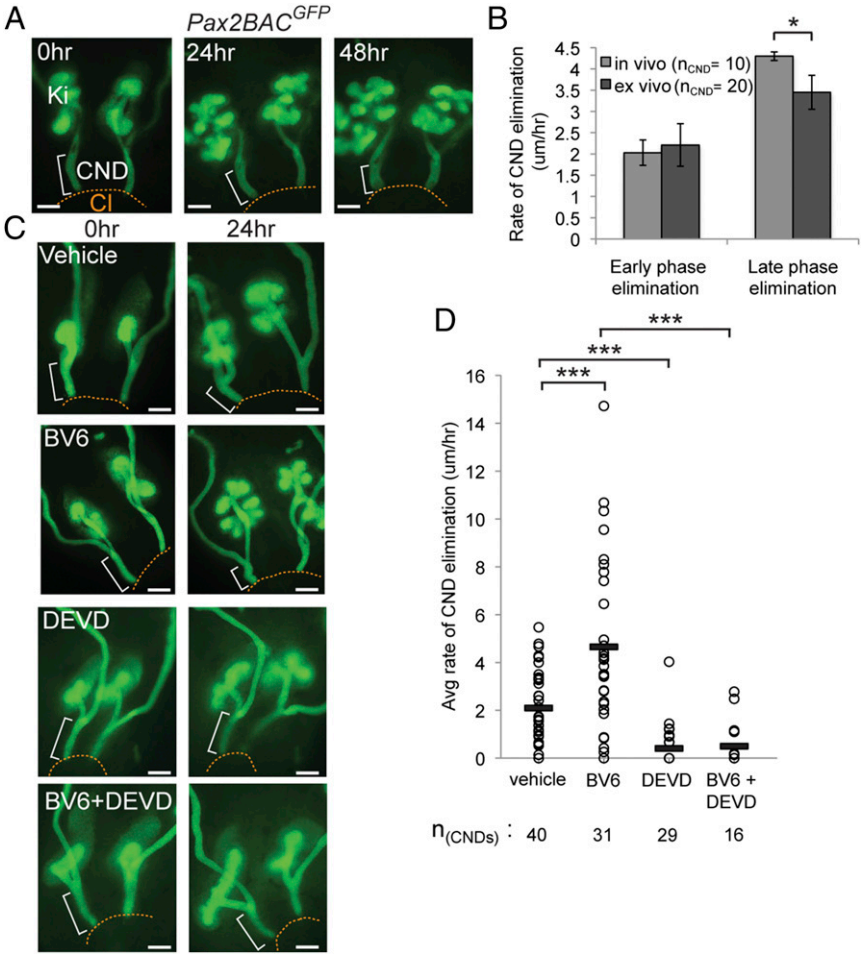

Fig. 2. Apoptotic elimination of the common nephric duct (CND) in ex vivo cultures is dampened by cIAP activity. (*A*) Ex vivo urogenital system culture recapitulates embryonic CND elimination. Representative time-lapse imaging of E11.5 *Pax2BAC*^{GFP} transgenic urogenital systems cultured for 24 h or 48 h shows the progressive disappearance of the CND (white bracket in *A*) relative to the cloaca (Cl). Ki, kidney. (*B*) Quantification of the rate of CND elimination in ex vivo cultures mirrors the in vivo rate between E11.5 and E12.5 (ex vivo 0–24 h; early phase) and E12.5 and E13.5 (ex vivo 24–48 h; late phase). (C) CND elimination in ex vivo cultures is accelerated by the cIAP1,2 inhibitor BV6 and both WT and BV6-mediated acceleration requires caspase 3,7-dependent apoptosis as shown by z-DEVD-fmk (DEVD) treatment. (*D*) Quantification of CND elimination rate by time-lapse imaging of ex vivo cultures cotreated with small molecule inhibitors BV6 and z-DEVD-fmk for 24 h demonstrates that CND elimination is accelerated by cIAP1,2 inhibition (BV6) in a caspase 3,7-dependent manner (DEVD). (Scale bars in *A* and *C*, 100 μm.) *P* values are calculated using Student's *t* test (*B*) and one-way ANOVA (*D*). All error bars indicate SEM. $*P < 0.05$, $***P < 0.005$.

Whole-mount immunofluorescence of ex vivo cultures revealed a normal gradient of cleaved caspase 3 in the WT CND, which was absent from vehicle-treated *Ptprs*$^{-/-}$; *Ptprf*$^{-/-}$ urogenital systems (Fig. 3*A*), as previously reported (7). Remarkably, BV6 treatment of *Ptprs*$^{-/-}$; *Ptprf*$^{-/-}$ ex vivo cultures restored normal levels of apoptosis in the CND (Fig. 3*A*), suggesting that IAPs act to restrict apoptosis downstream of LAR-RPTPs in the CND.

Quantititive PCR (qPCR) analysis and whole-mount in situ hybridization of WT E11.5 embryos revealed strong *Birc2* (cIAP1) expression specifically in the nephric duct, whereas *Birc3* (cIAP2) expression was weak and diffuse (*SI Appendix*, Fig. S2). To determine whether cIAP1 acts as a mediator of LAR-RPTP activity in the CND, we performed a genetic rescue of *Ptprs*$^{-/-}$; *Ptprf*$^{-/-}$ embryos by inactivation of the cIAP1 gene *Birc2* (*Ptprs*$^{-/-}$; *Ptprf*$^{-/-}$; *Birc2*$^{-/-}$ embryos). In striking contrast to the strong apoptotic deficiency observed in *Ptprs*$^{-/-}$; *Ptprf*$^{-/-}$ embryos, both cleaved caspase 3 and TUNEL signals were fully restored in *Ptprs*$^{-/-}$; *Ptprf*$^{-/-}$; *Birc2*$^{-/-}$ CNDs (Fig. 3 *B*–*D*). From these results, we conclude that LAR family phosphatases regulate CND apoptosis through cIAP1 activity.

LAR Family Phosphatases Promote cIAP1 Degradation During Apoptosis. To further elucidate the molecular regulation of cIAP1 by LAR-RPTPs, we first asked if the catalytic activity of the phosphatases was necessary for apoptotic cell death modulation. As expected, WT MEFs transfected with an empty vector were sensitive to cisplatin-mediated apoptosis, while those deficient for LAR-RPTPs (TKO) were resistant, as measured by caspase 3,7 activity (Fig. 3*E*). Reintroduction of the mCherry-tagged full-length *Ptprs* (RPTPσ) into TKO MEFs was able to completely restore the sensitivity to apoptotic stimuli (Fig. 3*E*). Importantly, this function was dependent on phosphatase activity as both the Asp to Ala (D/A) and Cys to Ser (C/S) catalytically dead mutants of RPTPσ failed to fully rescue the survival phenotype (Fig. 3*E*). To determine if cIAP1 and LAR-RPTPs are part of a common complex, we next expressed a full-length FLAG-tagged cIAP1 with either a WT (GST-RPTPσ) or the catalytic-mutant GST-tagged RPTPσ$_{D/A}$ phosphatase domain in HEK293 cells. GST pulldown of RPTPσ revealed a molecular interaction between the phosphatase and endogenous cIAP1 in both cisplatin- or vehicle-treated conditions (Fig. 3*F*). Of note, the interaction between FLAG-cIAP1 and GST-RPTPσ$_{D/A}$ was strengthened compared with the WT GST-RPTPσ (Fig. 3*F*),

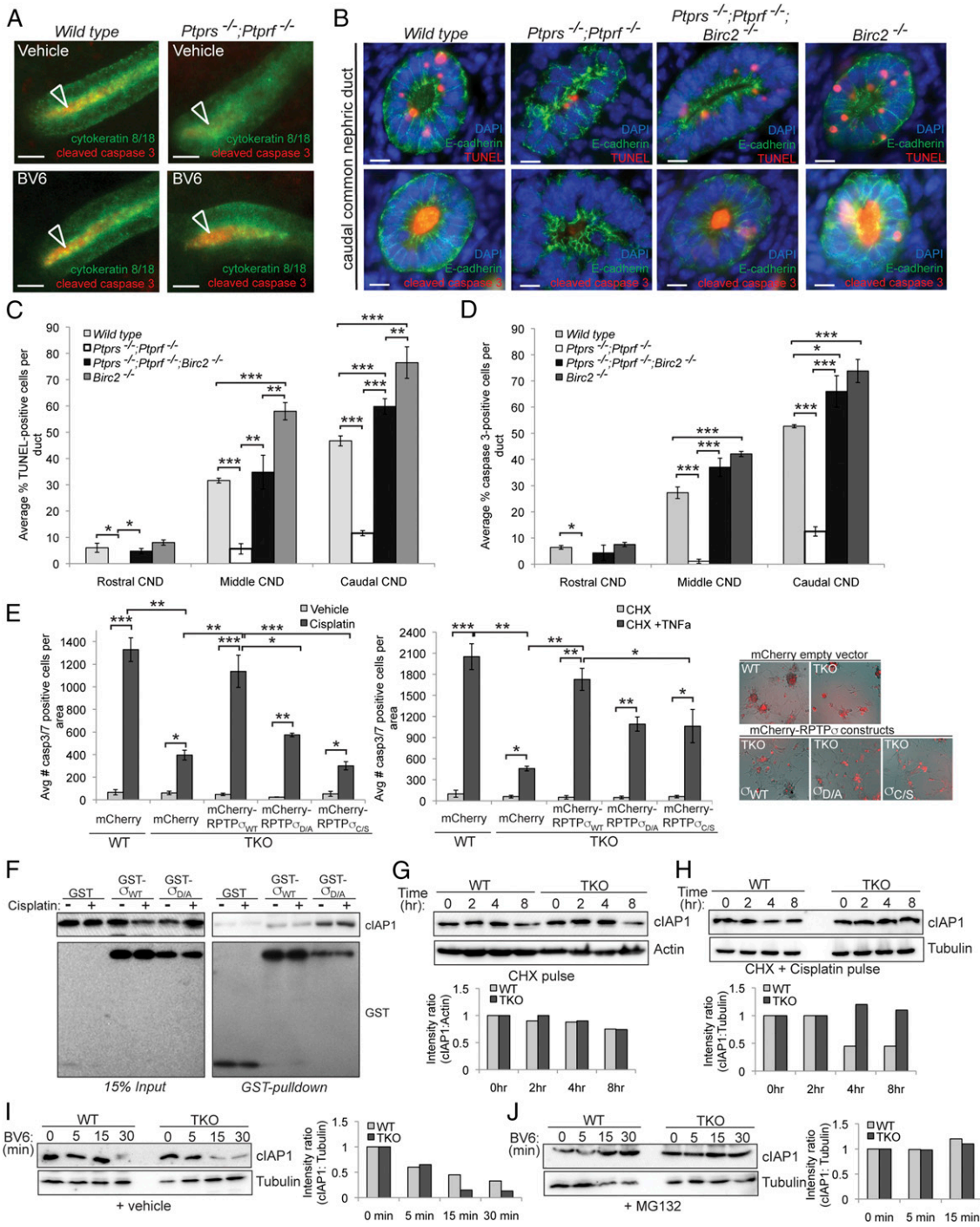

Fig. 3. cIAP1 acts downstream of LAR-RPTPs during apoptosis-mediated common nephric duct (CND) elimination. (*A*) BV6 treatment restores apoptosis in LAR family-deficient CNDs. Whole-mount immunofluorescence for cytokeratin 8/18 and cleaved caspase 3 (white arrowhead) on WT ($n = 12$ CNDs) and *Ptprs*$^{-/-}$*; Ptprf*$^{-/-}$ ($n = 10$ CNDs) urogenital ex vivo cultures treated with vehicle or BV6 for 20 h. (*B*) Genetic rescue of *Ptprs*$^{-/-}$*; Ptprf*$^{-/-}$ CND apoptosis by gene inactivation of *Birc2* (cIAP1) ($n = 6$ CNDs per genotype). Section immunofluorescence of the caudal CND region (adjacent to the cloaca) stained for DAPI, E-cadherin, and TUNEL or cleaved caspase 3. (*C* and *D*) Quantification of apoptotic rates in *Ptprs; Ptprf; Birc2* allelic series from *B*, stained for TUNEL (*C*) or cleaved caspase 3 (*D*). Results were quantified at three levels along the CND (rostral, middle, and caudal) with rostral being adjacent to the ureter branch point and caudal adjacent to the cloaca (bladder primordium). (*E*) Caspase 3,7 activity measured by fluorogenic substrate following transient expression of the mCherry-tagged full-length RPTPσ$_{WT}$ or the catalytic mutants RPTPσ$_{D/A}$ and RPTPσ$_{C/S}$ in *Ptprs; Ptprf; Ptprd* triple knockout (TKO) MEFs compared with mCherry-tag expression in WT MEFs in response to cisplatin or TNFα and cycloheximide (CHX). This experiment shows a full rescue of the apoptotic phenotype with RPTPσ$_{WT}$ but not with the catalytic mutants. (*F*) Immunoblot showing an interaction between endogenous cIAP1 and the GST-tagged RPTPσ$_{WT}$ or RPTPσ$_{D/A}$ phosphatase domains. Lysate was coimmunoprecipitated for the GST tag and cIAP1 to assess the interaction. (*G* and *H*) Pulse-chase experiments assessing cIAP1 stability in the presence of cycloheximide alone (*G*) or cyclohexamide and cisplatin (*H*) over the indicated time period in WT versus TKO MEFs. Quantification of normalized cIAP1 band intensity is shown below. (*I* and *J*) A total of 2 μM BV6 stimulation in WT and TKO MEFs shows cIAP1 degradation within minutes in both WT and TKO cells (*I*), which is proteasome dependent (*J*), indicating a normal catalytic activity of cIAP1. Quantification of normalized cIAP1 band intensity is shown below. [Scale bars, 25 μm (*A*) and 5 μm in (*B*).] All cell experiments are representative of three independent experiments, performed in technical triplicates. All *P* values are calculated using one-way ANOVA. All error bars indicate SEM. $*P < 0.05$, $**P < 0.01$, $***P < 0.005$.

characteristic of substrate binding (23). Collectively these results suggest a direct regulation of cIAP1 activity by LAR family phosphatases during apoptosis.

To further investigate the mechanistic consequences of cIAP1 interaction with LAR-RPTPs, we examined cIAP1 stability under basal and apoptotic conditions. In both WT and TKO fibroblasts, the turnover of cIAP1 in the absence of de novo translation averages about 8 h under basal conditions (Fig. 3*G*). In control MEFs undergoing apoptosis, the half-life of cIAP1 is reduced to about 4 h (Fig. 3*H*). Strikingly, however, in the absence of LAR-RPTPs this half-life is prolonged more than twofold (Fig. 3*H*). To assess whether the increase in cIAP1 stability in the TKO MEFs results from defective autoubiquitination, we treated MEFs with the Smac-mimetic BV6 to induce cIAP1 dimerization, autoubiquitination, and proteosome-dependent degradation. Notably, BV6 stimulation rapidly induced cIAP1 degradation in both WT and TKO fibroblasts (Fig. 3*I*), which was prevented by addition of the proteosome inhibitor MG132 (Fig. 3*J*), indicating that LAR phosphatases do not affect cIAP1's E3-ligase activity.

Together, these results indicate that LAR family phosphatases promote cIAP1 proteasome-mediated degradation, thereby enhancing apoptotic progression.

cIAP1 Acts as Modulator of Ureter Maturation. The identification of cIAP1 as an intermediary in the regulation of apoptosis by LAR family phosphatases at both the genetic and molecular levels suggested a specific role for cIAP1 during ureter maturation. Detailed examination of *Birc2*$^{-/-}$ embryos indeed revealed a marked increase in the percentage of both cleaved caspase 3 and TUNEL-positive cells above WT levels (Fig. 4 *A* and *B*). Interestingly, the range of the rostro–caudal gradient of apoptosis was maintained in these embryos, but its slope was increased (Fig. 4*B*), consistent with a sensitization to apoptotic induction rather than a background increase in cell death. To determine the level at which cIAP1 acts in the apoptotic pathway, we performed immunofluorescent staining for cleaved caspases 8 and 9 across the CND, as a proxy for activator caspase activation. Both caspases showed a rostral–caudal gradient of activation in WT embryos, similar to that described for caspase 3 (Fig. 4 *A* and *B*). However, neither was affected by loss of *Birc2* (Fig. 4 *A* and *B*), consistent with a role for cIAP1 activity downstream of caspases 8 and 9. We next assessed whether cIAP1 acts in concert with XIAP, which has been more closely associated with effector caspase regulation (24, 25). However, the analysis of *Birc4*$^{-/-}$ (XIAP) mutant embryos showed no impact on CND apoptosis, as assessed by TUNEL staining (Fig. 4 *C* and *D*), thereby confirming cIAP1 as the main regulatory IAP in this system. To further understand the regulation of CND apoptosis by IAPs, we asked whether the cIAP1 inhibitory molecule Smac had an opposite effect to *Birc2* (cIAP1) in this system. Measuring the apoptotic levels in *Smac*$^{-/-}$ CNDs by both TUNEL and cleaved caspase 3 revealed a significant, though limited, decrease in the rate of apoptosis in the caudal region (Fig. 4 *E* and *F*). Here again the background level of apoptosis was unaffected, while the slope of the apoptotic gradient was reduced, consistent with a decrease in cell sensitivity to apoptotic induction. CND length was also found comparable to WT at E11.5, suggesting normal ureter budding and initiation of the maturation process (*SI Appendix*, Fig. S3*C*). To determine whether other IAP antagonists could compensate for the loss of Smac in the CND, we assessed the mRNA levels of *HtrA2*, *Arts*, and *Xaf1* (26–28). This analysis showed no change in HtrA2 and low to no expression of the XIAP antagonists Arts and Xaf1 in this system (*SI Appendix*, Fig. S3*D*).

Collectively, these results identify Smac-cIAP1 as an important module in the molecular cascade regulating the rate of apoptotic cell death during urinary tract morphogenesis.

Apoptotic Defects of Birc2 Mutant Mice Lead to Vesicoureteral Reflux. Vesicoureteral reflux is a pediatric disease affecting 1–2% of newborns and characterized by retrograde urine flow leading to renal damage and frequent urinary tract infections (29, 30). Previous mechanistic explanations for this disease have focused on the position of ureter budding, leading to misplaced ureters in the bladder wall (29–32), but we found ureter budding unaffected in *Birc2*$^{-/-}$ embryos (*SI Appendix*, Fig. S3 *A* and *B*). As an alternative possibility, we hypothesized that an increase in CND apoptosis would lead to an acceleration in ureter maturation and a mispositioning of the ureter in the bladder wall.

To visualize the rate of duct elimination, we turned to ex vivo cultures using *Pax2BAC*^{GFP} embryos either WT or mutant for *Birc2*. Similar to the observations made using BV6 treatment, genetic inactivation of cIAP1 resulted in a twofold increase in the rate of CND elimination that was completely blocked by addition of the caspases 3,7-inhibitor z-DEVD-fmk (Fig. 5 *A* and *B*). Addition of z-LEHD-fmk and z-IETD-fmk to inhibit caspases 9 and 8, respectively, also resulted in a delay in ureter maturation in both control and *Birc2*-deficient animals (Fig. 5 *A* and *B*), suggesting the presence of an extrinsic signal acting either through or in parallel with mitochondrial permeabilization.

To determine whether the increased elimination speed led to ureter mispositioning, we used 3D optical tomography imaging to visualize ureter entry point in dissected urogenital systems from newborn control or *Birc2*-deficient pups. In contrast to the symmetrical positioning observed in WT animals, *Birc2*$^{-/-}$ pups consistently had at least one laterally displaced ureter insertion point (Fig. 5 *C* and *D* and *SI Appendix*, Fig. S4*D*). Congruent with the misplaced insertions, *Birc2*$^{-/-}$ pups showed dilated (but structurally normal) ureters (Fig. 5*E* and *SI Appendix*, Fig. S4 *A* and *H*), angled ureterovesical junctions (*SI Appendix*, Fig. S4*E*), and slightly shorter intravesical ureter lengths (*SI Appendix*, Fig. S4*C*) characteristic of vesicoureteral reflux (29–32).

To assess VUR, we used a surrogate of hydrostatic pressure to determine the sensitivity to ureter reflux (31, 32). These experiments were done in a pure C57BL/6 genetic background known to be completely resistant to vesicoureteral reflux (32). Accordingly, none of the control mice refluxed in this assay (Fig. 5 *F* and *G* and *SI Appendix*, Fig. S4*F*). In contrast, half of the *Birc2*$^{-/-}$ mice harbored vesicoureteral reflux, with an equal proportion refluxing unilaterally or bilaterally (Fig. 5 *F* and *G* and *SI Appendix*, Fig. S4*F*). Interestingly, most of the reflux observed in *Birc2*$^{-/-}$ animals occurred close to voiding pressure (*SI Appendix*, Fig. S4 *E* and *F*), which models the phenotype observed in human patients (29, 30). In line with the unaffected rate of apoptosis observed in *Birc4* (XIAP)-deficient animals, these failed to show a reflux phenotype in this assay (Fig. 5 *F* and *G*). From these results, we conclude that increased CND apoptosis, such as that observed in *Birc2*-deficient animals, can result in accelerated ureter maturation leading to displaced ureter insertion and vesicoureteral reflux.

Discussion

Morphogenetic apoptosis, the process by which apoptotic cell death drives the reorganization of a developing tissue, is crucial for embryonic development (1–4). However, the precise regulatory mechanisms governing apoptosis during development are largely unknown, especially with respect to the relative sensitivity of cells to apoptotic cell death. We and others have previously described the process of ureter maturation by morphogenetic apoptosis, and the requirement of LAR-RPTPs in this process (6–8). Here we show that LAR-RPTPs act by antagonizing the cIAP1 to modulate the rate of ureter maturation. cIAP1 activity is required as an apoptotic brake, slowing the response of CND cells to caspase 3-dependent apoptotic cell death. This permissive regulatory pathway acts as a modulator of cellular sensitivity to apoptotic triggers during development.

Using mouse models, we find that pharmacological or genetic inactivation of *Birc2* (cIAP1) is sufficient to fully rescue the severe apoptotic deficit found in the CND of mice lacking the LAR family phosphatases, *Ptprs* and *Ptprf* (7), thus placing LAR-RPTPs upstream of cIAP1 activity. This finding demonstrates

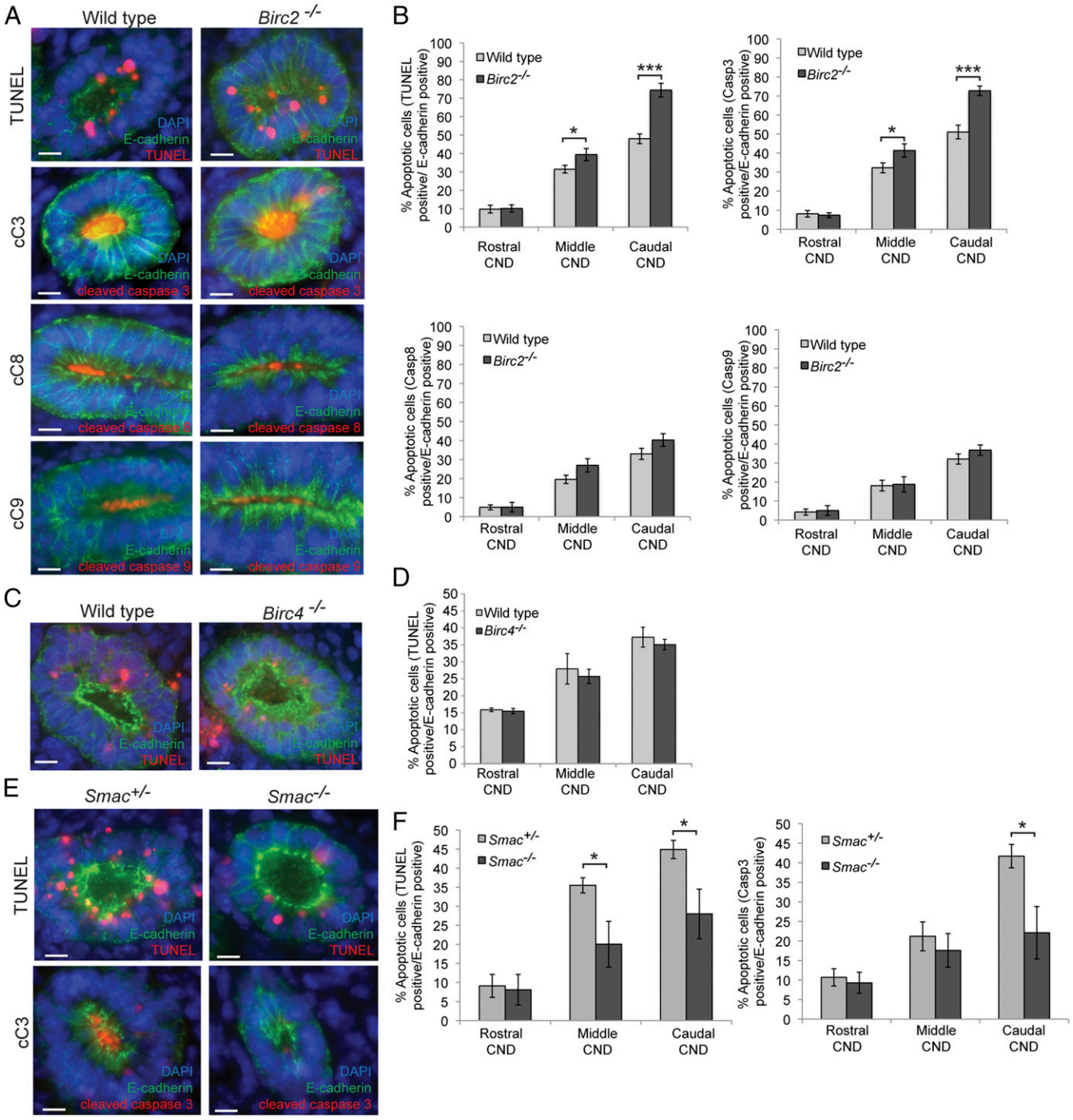

Fig. 4. cIAP1 modulates the rate of apoptotic cell death during common nephric duct (CND) elimination. (*A*) Representative section immunofluorescence of WT or *Birc2*$^{-/-}$ caudal CND stained for TUNEL, cleaved caspase 3 (cC3), cleaved caspase 8 (cC8), or cleaved caspase 9 (cC9) and costained for DAPI and E-cadherin. (*B*) Quantification of apoptotic rates across the CND from WT or *Birc2* mutant stainings ($n = 20$ CNDs per genotype) reveals an increase in caspase 3 and TUNEL positive cells but unaffected rates of cleaved caspase 8 and 9 upon loss of cIAP1. (*C*) Representative section immunofluorescence from the caudal CND (adjacent to the cloaca) from WT ($n = 8$ CNDs) and *Birc4* mutant ($n = 10$ CNDs) E11.5 embryos costained for TUNEL, E-cadherin, and DAPI. (*D*) Quantification of apoptotic rates across the length of the CND fails to show any effect for *Birc4*. (*E*) Representative section immunofluorescence from the caudal CND (adjacent to the cloaca) from *Smac* heterozygous ($n = 6$ CNDs) and mutant ($n = 6$ CNDs) E11.5 embryos costained for TUNEL or cleaved caspase 3, E-cadherin, and DAPI. (*F*) Quantification of apoptotic rates across the length of the CND by TUNEL or cleaved caspase 3 shows a reduction in apoptosis upon loss of *Smac*. (Scale bars in *A*, *C*, and *E*, 5 μm.) All *P* values are calculated using one-way ANOVA. All error bars indicate SEM. $*P < 0.05$, $***P < 0.005$.

that cIAP1 is a critical component of the signaling pathway linking LAR family phosphatases to the modulation of apoptotic cell death. Accordingly, *Birc2*-deficient mice show increased CND apoptosis, resulting in accelerated ureter maturation and vesicoureteral reflux. Of note, this is a unique developmental phenotype reported for *Birc2*$^{-/-}$ mice.

Our genetic analysis further reveals that mice mutant for the cIAP1 antagonist Smac show a partial reduction in CND apoptosis,

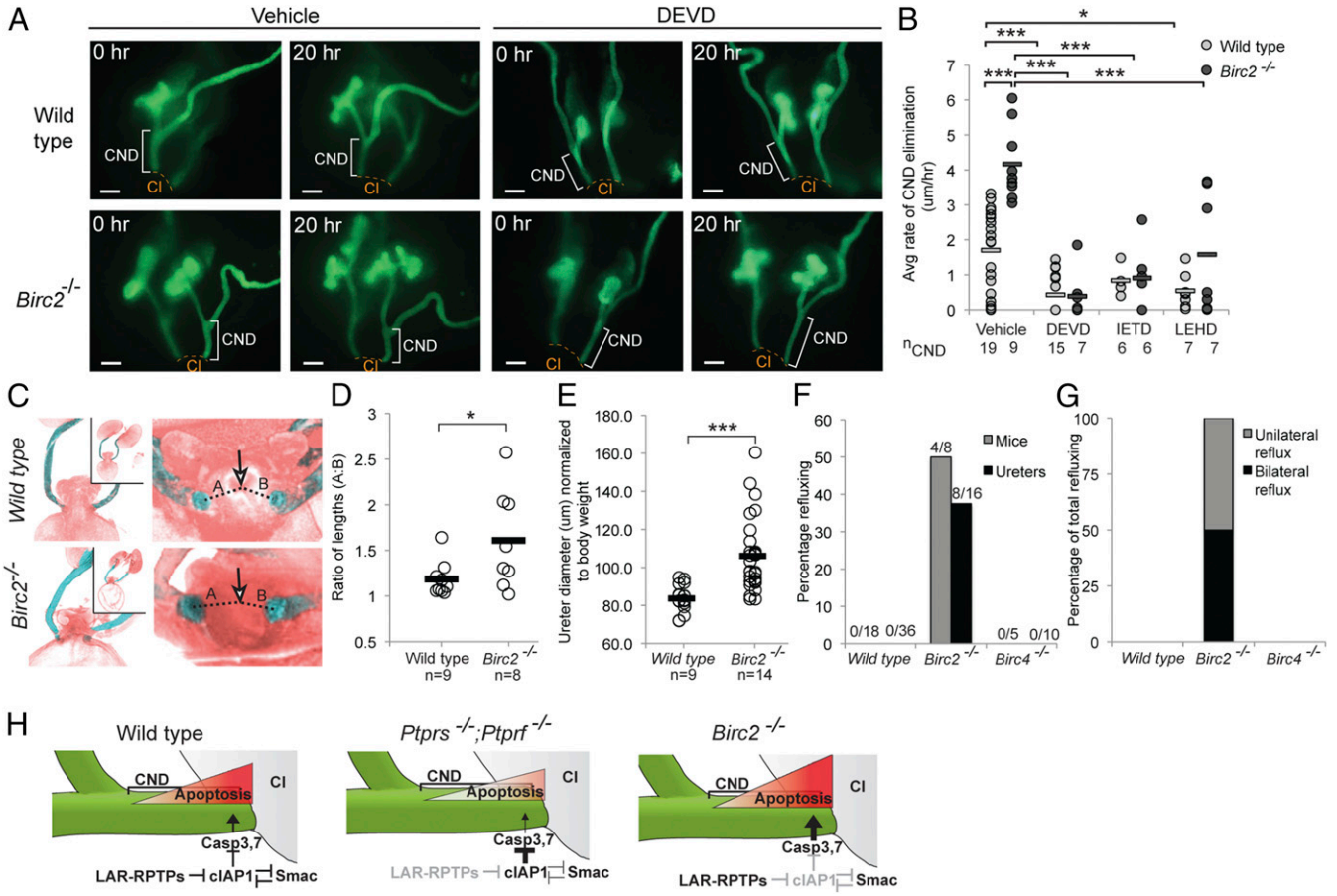

Fig. 5. Apoptotic defects in cIAP1 mutant mice are associated with vesicoureteral reflux. (*A*) Representative ex vivo urogenital cultures of E11.5 *Pax2BAC*^{GFP} transgenic animals either WT or mutant for *Birc2* followed by time-lapse imaging for 20 h. (*B*) Quantification of CND elimination in WT and *Birc2*$^{-/-}$ ex vivo cultures treated with inhibitors for caspase 3/7 (DEVD), caspase 8 (IETD), or caspase 9 (LEHD) suggests a role for both extrinsic and intrinsic pathways. (*C*) Representative optical tomography 3D images of WT and *Birc2*-mutant urogenital systems at postnatal day 0 in front view (*Left*) and from inside bladder (*Right*). Ureters are cyan; arrow indicates urethral opening; and lines A and B represent distance to ureter insertion points. (*D*) Quantification of ureter insertion point ratios (lines A and B in *A*) of control and *Birc2*$^{-/-}$ pups based on optical tomography imaging show an increased variability in ureter positioning in mutants. (*E*) Dilation of *Birc2*-null postnatal day 0 ureters compared with control pups measured from dissected urogenital systems and normalized to body weight. (*F* and *G*) Ink injection assay measuring the frequency (*F*) and laterality (*G*) of vesicoureteral reflux on postnatal day 0 control, *Birc2*$^{-/-}$, and *Birc4*$^{-/-}$ pups show a *Birc2*-specific reflux phenotype. (*H*) Model of apoptotic regulation by the LAR-RPTPs–cIAP1 axis to control CND elimination. (Scale bars, 100 μm in *A*.) *P* values are calculated using one-way ANOVA in *B* and using Mann–Whitney *u* tests in *D*–*G*. $*P < 0.05$, $***P < 0.005$.

which is the expected opposite to the *Birc2*-mutant phenotype. This is remarkable as *Smac* mutant mice were previously reported to be devoid of both developmental and adult phenotypes (33). The observed reduction in apoptosis is not sufficient to generate an overt developmental phenotype. Importantly, however, the strong reduction of apoptosis observed in *Ptprs*$^{-/-}$*; Ptprf*$^{-/-}$ animals leads to vesioureteral junction obstruction in only 50% of animals (7), thereby highlighting the morphogenetic plasticity of this system in buffering against disruptions in apoptotic regulation. Notably, these results also suggest that LAR family phosphatase regulation of cIAP1 is a predominant force in restricting morphogenetic apoptosis of the CND, while Smac appears to play an indirect or modulatory role.

Our work identifies a role for LAR-RPTPs in apoptotic modulation downstream of MOMP in both intrinsic and extrinsic pathways. In support of this, activation of upstream caspases 8 and 9 was indeed unaltered in LAR-RPTP–deficient CNDs in vivo (7) and in MEFs. Similarly, tBid activation and subsequent Smac release were unaffected upon apoptotic stimulation. Finally, LAR-RPTP–deficient MEFs were refractory to mitochondrial apoptotic activation by ABT-737/obatoclax, consistent with a regulatory role downstream of MOMP.

In line with these findings, *Birc2*-mutant mice showed altered caspase 3 and TUNEL levels, but harbored normal caspase 8 and caspase 9 activation levels in the CND. In this context, it is interesting that the ureter maturation phenotype was specifically observed in the absence of *Birc2*, while *Xiap*-deficient mice failed to show any apoptotic or developmental phenotype in this system. XIAP has indeed been more closely associated with the regulation of caspase 3 activity, while cIAPs are generally thought to act upon TNF receptor activity in promoting cell survival during inflammation and cancer (20, 24, 34–36). However, evidence suggests a role for cIAPs in regulating caspase 3 activity as they can directly interact with effector caspases 3 and 7 and promote their ubiquitination and proteasomal degradation through their E3-ligase activity. In addition *Xiap*-deficient mice show only minor apoptosis-related phenotypes, which was proposed to result from the compensatory up-regulation of cIAP1/2 (33, 37). Although the details of apoptosis regulation downstream of cIAP1 function in the urinary tract remains to be fully elucidated, it is possible that, in a developmental context, cIAP1 exerts a regulatory activity at the level of effector caspases that is revealed by the specific role of LAR-RPTPs downstream of MOMP.

At the molecular level, our results point to a simple model by which LAR phosphatase activity differentially regulates the stability of cIAP1 leading to an increased apoptotic response downstream of mitochondrial membrane permeabilization (Fig. 5*H*). Upon loss of LAR-RPTP function, cIAP1 stability is prolonged by more than twofold, specifically under apoptotic conditions. The fact that BV6 can effectively induce cIAP1 degradation in TKO cells further suggests that RPTPs do not directly affect cIAP1 E3-ligase activity or downstream proteasome degradation potential but instead provide a regulatory signal affecting upstream regulators of cIAP1 degradation such as Smac and other IAP antagonists (38–43).

Another important observation emerging from this study is that the increased apoptotic rate found in *Birc2* (cIAP1) mutant urinary tracts can lead to vesicoureteral reflux in newborn mice. This previously unappreciated link between vesicoureteral reflux and apoptosis identifies a candidate pathway to be explored for this common but poorly understood disease (21, 29, 30, 44). Together with the demonstration that the apoptotic deficiency seen in LAR-RPTP–deficient animals can lead to ureter obstruction (7), this result points to an exquisite system by which the fine regulation of apoptotic cell response is required to properly position the ureter, while too much or too little apoptosis leads to a disease state (Fig. 5*H*). Together these observations reveal that the rate of cellular apoptosis is able to control a temporal clock required for appropriate tissue morphogenesis, which contrasts to the less nuanced cell clearance view of apoptosis commonly taken.

Collectively, these results identify cIAP1 as a central modulator of morphogenetic apoptosis in the urinary tract. They further identify a regulatory signal modulating the cellular response to terminal apoptosis. Imbalances or mutations in this regulatory system may lead to congenital anomalies of the urinary tract and other apoptosis-related diseases.

Materials and Methods

Mice. The derivation of *Ptprs; Ptprf*, *Birc2*, *Birc4*, and *Smac* mice have been previously described (7, 45, 46). *Pax2BAC*^{GFP} transgenic animals (47) were used to visualize the renal lineage. Genetic rescue experiments were performed by crossing triple heterozygous *Ptprs; Ptprf; Birc2* animals generated from the individual strains. Derivation of the *Ptprs; Ptprf; Ptprd* animals used to generate TKO MEF lines will be described elsewhere. Animals were housed under pathogen-free conditions in the McGill University Animal Resource Centre. Timed matings were performed and detection of a copulatory plug was taken at embryonic day 0.5 (E0.5). Animal experiments for this study were approved by the McGill Animal Care Committee, and were conducted in compliance with the Canadian Council of Animal Care ethical guidelines.

Cell Culture. MEF lines were derived from four control and four independent *Ptprs; Ptprf; Ptprd* TKO embryos at E14.5 following standard procedures, as described previously (48). MEFs and human embryonic kidney 293T (HEK293T) cells were maintained in DMEM (Wisent) supplemented with 10% FBS (Gibco) and penicillin–streptomycin (Invitrogen). All MEF experiments were done at passage 5. Before induction of apoptosis, cells were serum starved for 1 h and subsequently treated with 100 μM cisplatin, 50 μM etoposide, 10 ng/mL cycloheximide, and 1 ng/mL TNFα (all from Sigma), 2 μM obatoclax (a kind gift from G. Shore, McGill University, Montreal), or 10 μM ABT-737 (Cedarlane) in serum-free media for the indicated time period. BV6 (a kind gift from Genentech, San Francisco) was used at 2 or 5 μM as indicated. For experiments involving proteosome inhibition, cells were pretreated with 10 μM MG132 (Calbiochem) for 4 h before apoptotic stimulation. Pan-caspase inhibitor z-VAD-fmk (Cedarlane) and caspase 8 and 9 inhibitors z-IETD-fmk and z-LEHD-fmk (Santa Cruz Biotechnology) were added with apoptotic triggers at a concentration of 1 μM. Caspase 3,7 activity was assessed using the Cell Player caspase 3,7 fluorogenic substrate (Essen BioScience) following manufacturer's instructions, and fluorescence was tracked using the Incucyte FLR live imaging system (Essen BioScience). Transient transfection of expression constructs in MEFs was achieved using the Nucleofection system (Lonza) following the manufacturer's procedure. Expression was allowed to proceed for 24 h before collection of cell lysates. Expression of constructs in the HEK293T cell line was performed using PolyJet DNA Transfection reagent (FroggaBio) and allowed to proceed for 24 h before lysate collection.

Expression Constructs. Generation of the full-length FLAG-tagged cIAP1, Smac-dsRED, mCherry-tagged RPTPσ WT and catalytic mutants (D/A and C/S), and the GST-tagged intracellular domain of RPTPσ WT and catalytic mutant (D/A) mammalian expression constructs have been previously described (49–51).

Immunoblotting and Immunoprecipitation. Cells were treated with the indicated chemicals and then rinsed with PBS, scraped, and lysed with FLAG lysis buffer (50 mM Tris·HCl, pH 7.4, 150 mM NaCl, 1 mM EDTA, 1% Triton X-100) containing EDTA-free Complete Protease Inhibitors (Roche) for 30 min on ice. Protein concentration was determined by Bradford assay (Bio-Rad), and 10–50 μg of protein was loaded on SDS/PAGE gels and run following standard procedures. Protein was transferred to PDVF membranes and blotted using standard procedures. Primary and secondary antibody dilution and blocking followed manufacturer's recommendations. Antibodies used were mouse anti-GST (Abgent); rabbit anti-caspase 3 (Millipore); rabbit anti-cleaved caspase 3 (D175), rabbit anti-cleaved caspase 8 (D387), rabbit anti-cleaved caspase 9 (D353), and mouse anti-caspase 9 (all Cell Signaling Technology); rabbit anti-tubulin, rabbit anti-cIAP1, and rabbit anti-truncated Bid (all Abcam); and mouse anti-Smac (BD Biosciences). Secondary antibodies were HRP-conjugated anti-rabbit (Cell Signaling Technology) and HRP-conjugated anti-mouse (GE Healthcare) antibodies, which were detected with enhanced chemilumiscent reagent (Millipore) following manufacturer's instructions. Luminescence was captured either by film, or using the FluorChem HD2 imaging system (Cell Biosciences). Western blot band intensities were assessed using ImageJ software. Cells for protein-interaction analysis were prepared as described above, and equal amounts of lysate were immediately incubated with glutathione-agarose beads (Thermo Fisher) for 4 h at 4 °C. Following washes with FLAG-lysis buffer, protein complexes were eluted using Laemelli loading buffer and boiled before loading on SDS/PAGE for analysis.

Ex Vivo Urogenital System Culture. The ex vivo culture system has been previously described (6, 52). Briefly, embryonic day 11.5 urogenital systems were dissected in PBS, rinsed with DMEM:F12 medium, and placed flat on a 0.45-μm nitrocellulose filter (Millipore) to be cultured at the air/media interface at 37 °C, 5% CO_2. Cultures were allowed to settle for 1 h before imaging and treatment with the indicated compounds. Caspase inhibitors z-DEVD-fmk (Enzo Life Sciences), z-IETD-fmk, and z-LEHD-fmk (Santa Cruz Biotechnology), and BV6 were used at a concentration of 10 μM. All compounds were diluted in DMEM:F12 media (Wisent) supplemented with 10% FBS (Gibco) and 1× penicillin–streptomycin (Invitrogen). The rate of CND elimination was assessed by time-lapse imaging using either a Zeiss AxioPlan 2 microscope or a Zeiss Lumar V12 stereomicroscope, and the length of the CND in micrometers was tracked using the curve spline measurement function at each time point. The rate of elimination was defined as the difference in CND starting and endpoint lengths over culture time.

Immunofluorescence and in Situ Hybridization. Cell culture and tissue samples for immunofluorescent and in situ hybridization staining were processed following standard procedures. Briefly, immunocytochemistry was done on cells grown on acid-treated coverslips until confluent before apoptotic induction. Following treatment, cells were fixed in 4% paraformaldehyde. Cells were permeabilized in PBS, 0.3% Triton X-100, 0.1% Tween-20 (permeabilization solution) for 2 min at room temperature, blocked with DAKO protein block (serum-free) solution for 1 h at room temperature, and incubated with mouse anti-Smac antibody (1:100; BD Biosciences) overnight. The following day, cells were incubated with goat anti-mouse Alexa Fluor-488 secondary antibody (1:400; Invitrogen) and counterstained with Alexa Fluor-546 conjugated phalloidin (1:400; Invitrogen) and DAPI (50 μg/mL; Invitrogen). For apoptotic index, cells were processed as above and stained by TUNEL (TMR-red In Situ Cell Death Detection Kit, Roche) and DAPI for 1 h at 37 °C. For tissue staining, embryos or dissected urogenital systems were fixed with 4% paraformaldehyde for 30 min at room temperature, and either processed directly or embedded in VWR clear frozen section compound and cryosectioned at 12 μm. Whole-mount in situ hybridization was performed as described (53). The *Pax2* probe has been previously reported (54). Probes corresponding to 900–1,796 nt and 406–1,335 nt of *Birc2* and *Birc3* were generated using T7-promoter containing PCR products. Whole-mount and section immunofluorescent stainings were permeabilized for 2 h or 5 min, respectively, using permeabilization solution and then blocked in DAKO protein block (serum-free) solution. Whole-mount urogenital systems were incubated with primary antibodies for cytokeratin 8/18 (1:100; Fitzgerald) and cleaved caspase 3 (1:100; Cell Signaling Technology) for 24–48 h.

Secondary antibody detection used goat anti-guinea pig Alexa Fluor-488 and anti-rabbit Alexa Fluor-568 (1:100; Invitrogen) overnight. Samples were washed a minimum of three times for 1 h each following each antibody incubation and mounted in SlowFade Gold mounting reagent (Invitrogen) for imaging. Sections were incubated with primary antibodies for cleaved caspase 3, cleaved caspase 8, and cleaved caspase 9 (1:100; Cell Signaling Technology), cytokeratin 8/18 (1:100; Fitzgerald), smooth muscle actin (1:500; Sigma), and E-cadherin (1:500; Invitrogen) overnight at 4 °C. Secondary antibody detection was performed using donkey anti-rat Alexa Fluor-488 and donkey anti-rabbit Alexa Fluor-568 antibodies (1:400; Invitrogen) and costained with DAPI. Alternatively, tissue sections were labeled by TUNEL using the In Situ Cell Death Detection Kit (Roche), following manufacturer's instructions. Sections were mounted in either Prolong or SlowFade mounting medium (Invitrogen) before imaging. Images were acquired on a Zeiss AxioPlan 2 microscope, a Zeiss LSM 5 Pascal/Axiovert 200 M confocal microscope, or a Zeiss LSM 710 AxioObserver confocal microscope (McGill University Life Sciences Complex Advanced BioImaging Facility). To assess the apoptotic index across the CND, sections were grouped into rostral (adjacent to the ureteric bud), middle, and caudal (adjacent to the cloaca) categories and counted (totaling ~500 cells per CND), as previously described (7).

Real-Time Quantitative PCR. Standard methods for reverse transcription and qPCR from dissected tissue samples were followed. Briefly, E11.5 urogenital systems were dissected, and placed in TRIzol for RNA extraction following the manufacturer's procedure. A total of 1 μg of RNA was used to generate cDNA by SuperScript III reverse transcriptase (Invitrogen) and random hexameric primers. qPCR was performed on Eppendorf Realplex2 cyclers using the iQ SYBR Green Supermix Kit (Bio-Rad). Quantitative PCR primers were designed against 751–878, nt 1,081–1,231 nt, 1,068–1,220 nt, and 973–1,159 nt of mouse *caspase 3*, *Birc2*, *Birc3*, and *Birc4*, respectively.

Vesicoureteral Reflux and Optical Tomography Imaging. The ink injection assay to assess vesicoureteral reflux has been previously described (31, 32, 55). Briefly, urogenital systems from postnatal day 0 pups were exposed from anesthetized and decapitated animals under a Zeiss Stemi 2000-C dissecting microscope. The bladder was punctured with a needle attached to a reservoir of dye starting from zero pressure (equal height with the bladder) and progressively raised. Bladder voiding height and the presence of dye refluxing into the ureters was tracked visually, and the height at which each occurs recorded as a proxy for pressure. Optical tomography 3D imaging was performed on dissected urogenital systems from postnatal day 0 pups following the manufacturer's protocol (Bioptonics Microscopy). Briefly, urogenital systems were fixed using 4% paraformaldehyde for 1 h at room temperature, and washed with PBS, before mounting in an agarose plug. The methanol-dehydrated agarose plug was cleared in benzyl alcohol:benzyl benzoate, before fixing to a magnetic mount and imaging. Images were captured in the eGFP channel, every 0.9°, and reconstructed using manufacturer's software (Bioptonics 3001 software suite). The length of the intravesicular ureters and the distance between urethral opening and ureter insertion points were calculated using 3D vector subtraction.

Analysis and Statistics. Statistical analyses using the Mann–Whitney *u* test, two-tailed Student's *t* tests, or one-way ANOVAs were performed using PRISM software. All error bars are presented as SE of measurement (SEM), and P values of <0.05 were considered significant. All experiments were performed a minimum of three times, and all animal analysis contains a minimum of $n = 3$ animals (which is six CNDs) per genotype. For statistical analysis, CNDs from individual animals were considered separate entities. Actual sample sizes are indicated in figures where appropriate.

ACKNOWLEDGMENTS. We thank Drs. Michel L. Tremblay, Junying Yuan, and Jochen H. M. Prehn for expression constructs; Drs. D. Vucic (Genentech), G. Shore, M. Saleh, and P. Barker (McGill University) for reagents; Dr. Mathieu Tremblay for experimental help; and members of the M.B. laboratory for critical reading of the manuscript. This work was supported by operating grants from the Kidney Foundation of Canada and the Canadian Institutes for Health Research (MOP-84343) (to M.B. and K.S.) and by studentships from the National Science and Engineering Research Council and the Fonds de Recherche du Québec-Santé.

1. Pérez-Garijo A, Steller H (2015) Spreading the word: Non-autonomous effects of apoptosis during development, regeneration and disease. *Development* 142: 3253–3262.
2. Meier P, Finch A, Evan G (2000) Apoptosis in development. *Nature* 407:796–801.
3. Baehrecke EH (2002) How death shapes life during development. *Nat Rev Mol Cell Biol* 3:779–787.
4. Miura M (2012) Apoptotic and nonapoptotic caspase functions in animal development. *Cold Spring Harb Perspect Biol* 4:a008664.
5. Batourina E, et al. (2002) Distal ureter morphogenesis depends on epithelial cell remodeling mediated by vitamin A and Ret. *Nat Genet* 32:109–115.
6. Batourina E, et al. (2005) Apoptosis induced by vitamin A signaling is crucial for connecting the ureters to the bladder. *Nat Genet* 37:1082–1089.
7. Uetani N, et al. (2009) Maturation of ureter-bladder connection in mice is controlled by LAR family receptor protein tyrosine phosphatases. *J Clin Invest* 119:924–935.
8. Kim ST, Ahn SY, Swat W, Miner JH (2014) DLG1 influences distal ureter maturation via a non-epithelial cell autonomous mechanism involving reduced retinoic acid signaling, Ret expression, and apoptosis. *Dev Biol* 390:160–169.
9. Caruana G, Bertram JF (2015) Congenital anomalies of the kidney and urinary tract genetics in mice and men. *Nephrology (Carlton)* 20:309–311.
10. Parrish AB, Freel CD, Kornbluth S (2013) Cellular mechanisms controlling caspase activation and function. *Cold Spring Harb Perspect Biol* 5:a008672.
11. Silke J, Vaux DL (2015) IAP gene deletion and conditional knockout models. *Semin Cell Dev Biol* 39:97–105.
12. Verhagen AM, et al. (2000) Identification of DIABLO, a mammalian protein that promotes apoptosis by binding to and antagonizing IAP proteins. *Cell* 102:43–53.
13. Du C, Fang M, Li Y, Li L, Wang X (2000) Smac, a mitochondrial protein that promotes cytochrome c-dependent caspase activation by eliminating IAP inhibition. *Cell* 102: 33–42.
14. Yang QH, Church-Hajduk R, Ren J, Newton ML, Du C (2003) Omi/HtrA2 catalytic cleavage of inhibitor of apoptosis (IAP) irreversibly inactivates IAPs and facilitates caspase activity in apoptosis. *Genes Dev* 17:1487–1496.
15. Hegde R, et al. (2002) Identification of Omi/HtrA2 as a mitochondrial apoptotic serine protease that disrupts inhibitor of apoptosis protein-caspase interaction. *J Biol Chem* 277:432–438.
16. Wu G, et al. (2000) Structural basis of IAP recognition by Smac/DIABLO. *Nature* 408: 1008–1012.
17. Liu Z, et al. (2000) Structural basis for binding of Smac/DIABLO to the XIAP BIR3 domain. *Nature* 408:1004–1008.
18. Chai J, et al. (2000) Structural and biochemical basis of apoptotic activation by Smac/DIABLO. *Nature* 406:855–862.
19. Dueber EC, et al. (2011) Antagonists induce a conformational change in cIAP1 that promotes autoubiquitination. *Science* 334:376–380.
20. Varfolomeev E, et al. (2007) IAP antagonists induce autoubiquitination of c-IAPs, NF-kappaB activation, and TNFalpha-dependent apoptosis. *Cell* 131:669–681.
21. Uetani N, Bouchard M (2009) Plumbing in the embryo: Developmental defects of the urinary tracts. *Clin Genet* 75:307–317.
22. Stewart K, Bouchard M (2014) Coordinated cell behaviours in early urogenital system morphogenesis. *Semin Cell Dev Biol* 36:13–20.
23. Flint AJ, Tiganis T, Barford D, Tonks NK (1997) Development of "substrate-trapping" mutants to identify physiological substrates of protein tyrosine phosphatases. *Proc Natl Acad Sci USA* 94:1680–1685.
24. Silke J, Meier P (2013) Inhibitor of apoptosis (IAP) proteins-modulators of cell death and inflammation. *Cold Spring Harb Perspect Biol* 5:a008730.
25. O'Riordan MX, Bauler LD, Scott FL, Duckett CS (2008) Inhibitor of apoptosis proteins in eukaryotic evolution and development: A model of thematic conservation. *Dev Cell* 15:497–508.
26. Martins LM, et al. (2004) Neuroprotective role of the Reaper-related serine protease HtrA2/Omi revealed by targeted deletion in mice. *Mol Cell Biol* 24:9848–9862.
27. Larisch S, et al. (2000) A novel mitochondrial septin-like protein, ARTS, mediates apoptosis dependent on its P-loop motif. *Nat Cell Biol* 2:915–921.
28. Liston P, et al. (2001) Identification of XAF1 as an antagonist of XIAP anti-Caspase activity. *Nat Cell Biol* 3:128–133.
29. Williams G, Fletcher JT, Alexander SI, Craig JC (2008) Vesicoureteral reflux. *J Am Soc Nephrol* 19:847–862.
30. Murawski IJ, Gupta IR (2008) Gene discovery and vesicoureteric reflux. *Pediatr Nephrol* 23:1021–1027.
31. Boualia SK, et al. (2011) Vesicoureteral reflux and other urinary tract malformations in mice compound heterozygous for Pax2 and Emx2. *PLoS One* 6:e21529.
32. Murawski IJ, et al. (2010) The C3H/HeJ inbred mouse is a model of vesico-ureteric reflux with a susceptibility locus on chromosome 12. *Kidney Int* 78:269–278.
33. Okada H, et al. (2002) Generation and characterization of Smac/DIABLO-deficient mice. *Mol Cell Biol* 22:3509–3517.
34. Rothe M, Pan MG, Henzel WJ, Ayres TM, Goeddel DV (1995) The TNFR2-TRAF signaling complex contains two novel proteins related to baculoviral inhibitor of apoptosis proteins. *Cell* 83:1243–1252.
35. Bertrand MJM, et al. (2008) cIAP1 and cIAP2 facilitate cancer cell survival by functioning as E3 ligases that promote RIP1 ubiquitination. *Mol Cell* 30:689–700.
36. Moulin M, et al. (2012) IAPs limit activation of RIP kinases by TNF receptor 1 during development. *EMBO J* 31:1679–1691.
37. Olayioye MA, et al. (2005) XIAP-deficiency leads to delayed lobuloalveolar development in the mammary gland. *Cell Death Differ* 12:87–90.
38. Tenev T, Zachariou A, Wilson R, Ditzel M, Meier P (2005) IAPs are functionally non-equivalent and regulate effector caspases through distinct mechanisms. *Nat Cell Biol* 7:70–77.

39. Zhuang M, Guan S, Wang H, Burlingame AL, Wells JA (2013) Substrates of IAP ubiquitin ligases identified with a designed orthogonal E3 ligase, the NEDDylator. *Mol Cell* 49:273–282.
40. Choi YE, et al. (2009) The E3 ubiquitin ligase cIAP1 binds and ubiquitinates caspase-3 and -7 via unique mechanisms at distinct steps in their processing. *J Biol Chem* 284:12772–12782.
41. Burke SP, Smith L, Smith JB (2010) cIAP1 cooperatively inhibits procaspase-3 activation by the caspase-9 apoptosome. *J Biol Chem* 285:30061–30068.
42. Eckelman BP, Salvesen GS (2006) The human anti-apoptotic proteins cIAP1 and cIAP2 bind but do not inhibit caspases. *J Biol Chem* 281:3254–3260.
43. Huang Hk, et al. (2000) The inhibitor of apoptosis, cIAP2, functions as a ubiquitin-protein ligase and promotes in vitro monoubiquitination of caspases 3 and 7. *J Biol Chem* 275:26661–26664.
44. Murawski IJ, Watt CL, Gupta IR (2011) Vesico-ureteric reflux: Using mouse models to understand a common congenital urinary tract defect. *Pediatr Nephrol* 26:1513–1522.
45. Conze DB, et al. (2005) Posttranscriptional downregulation of c-IAP2 by the ubiquitin protein ligase c-IAP1 in vivo. *Mol Cell Biol* 25:3348–3356.
46. Harlin H, Reffey SB, Duckett CS, Lindsten T, Thompson CB (2001) Characterization of XIAP-deficient mice. *Mol Cell Biol* 21:3604–3608.
47. Pfeffer PL, Payer B, Reim G, di Magliano MP, Busslinger M (2002) The activation and maintenance of Pax2 expression at the mid-hindbrain boundary is controlled by separate enhancers. *Development* 129:307–318.
48. Stewart K, Uetani N, Hendriks W, Tremblay ML, Bouchard M (2013) Inactivation of LAR family phosphatase genes Ptprs and Ptprf causes craniofacial malformations resembling Pierre-Robin sequence. *Development* 140:3413–3422.
49. Degterev A, et al. (2008) Identification of RIP1 kinase as a specific cellular target of necrostatins. *Nat Chem Biol* 4:313–321.
50. Rehm M, Düssmann H, Prehn JH (2003) Real-time single cell analysis of Smac/DIABLO release during apoptosis. *J Cell Biol* 162:1031–1043.
51. Chagnon MJ, et al. (2010) Receptor tyrosine phosphatase sigma (RPTPσ) regulates, p250GAP, a novel substrate that attenuates Rac signaling. *Cell Signal* 22: 1626–1633.
52. Batourina E, Gandhi D, Mendelsohn CL, Molotkov A (2012) Organotypic culture of the urogenital tract. *Methods Mol Biol* 886:45–53.
53. Grote D, et al. (2008) Gata3 acts downstream of beta-catenin signaling to prevent ectopic metanephric kidney induction. *PLoS Genet* 4:e1000316.
54. Adams B, et al. (1992) Pax-5 encodes the transcription factor BSAP and is expressed in B lymphocytes, the developing CNS, and adult testis. *Genes Dev* 6:1589–1607.
55. Murawski IJ, Watt CL, Gupta IR (2012) Assessing urinary tract defects in mice: Methods to detect the presence of vesicoureteric reflux and urinary tract obstruction. *Methods Mol Biol* 886:351–362.